Exact Solution for Functionally Graded Anisotropic Elastic Composite Laminates

E. PAN*
Department of Civil Engineering
The University of Akron
Akron, OH 44325-3905, USA

ABSTRACT: Exact solutions are derived for three-dimensional, anisotropic, linearly elastic, and functionally graded rectangular composite laminates under simply supported edge conditions. The solutions are expressed in terms of an elegant formalism that resembles the Stroh formalism, and the composite laminates can be made of multilayered functionally graded materials with their properties varying exponentially in the thickness direction. The present solution extends Pagano's solution to the functionally graded material, and can serve as a benchmark to the modeling of functionally graded composite laminates based on various numerical methods. Typical results of the present solution are discussed for a single functionally graded plate and a bi-layer plate with a functionally graded layer overlying a homogeneous layer. For both plates, a simple load is applied on their top surfaces. It is shown that with a suitable functionally graded layer, the tensile stress on the top surface (or the compressive stress on the bottom surface for a homogeneous layer overlying a functionally graded layer) of the bi-layer plate can be reduced. This interesting feature could be useful in the design of functionally graded composite laminates.

KEY WORDS: functionally graded material, composite laminate, anisotropic elasticity, exact three-dimensional solution, simply supported plate.

INTRODUCTION

ARTIFICIAL MATERIALS WITH multilayered structures, such as composite laminates, have been successfully applied to various material science and engineering fields. However, the mismatch of the material properties between the adjacent layers renders a stress concentration at the free edge, which has been long noticed to be the source for delamination and other failures (see e.g., [1–3]). In particular, when the conventional

* E-mail: pan2@akron.edu

0021-9983/03/21 1903–18 $10.00/0 DOI: 10.1177/002199803035565
© 2003 Sage Publications

thermal barrier coatings were used for high temperature applications, the mismatch of the thermal expansion coefficients between the coating and substrate materials may initiate debonding, delamination, and micro-cracks [4–6]. Thus, the functionally graded materials (FGMs) were introduced [7] to overcome the disadvantages associated with homogeneous coating materials and to reduce the residual stresses in layered composites by serving as tailored interfacial zone materials with continuously varying mechanical properties.

Owing to its special features with potential applications to many science and engineering fields, the FGM structure has attracted wide and increasing attentions of scientists and engineers in broad areas of research. So far, various numerical simulations have been carried out on the mechanical and fracture behaviors of such a structure [4,8–27]. Furthermore, certain analytical solutions have been also derived for FGMs. For instance, for geo-materials, such as soils and rocks where the elastic properties vary as a function of depth beneath the surface, Booker et al. [28] studied the static response of an isotropic elastic and inhomogeneous half-space subject to a line and point load, while Ben-Menahem [29] derived the Green's tensor and its potentials for the corresponding time-harmonic deformation. In other areas, Giannakopoulos and Suresh [30] studied the indentation on the surface of an FGM half space, and Kim and Noda [31] and Gray et al. [32] investigated the thermal conduction in FGMs. Very recently, Martin et al. [33] derived an analytical expression for the Green's function in anisotropic elastic FGMs where the material properties vary exponentially in a fixed direction, whilst Wang et al. [34] solved the symmetric problem of a point force in a transversely isotropic FGM half-space. Furthermore, for an FGM cylinder or disk, Horgan and Chan [35] derived an exact closed-form solution for the stress field and showed certain stress behaviors in the FGM cylinder; Vel and Batra [36], on the other hand, obtained the analytical solution for a simply supported multilayered FGM plate made of isotropic materials by using the Fourier series expansion method.

In this paper, we derive exact solutions for three-dimensional (3D), anisotropic elastic FGM (with exponentially varying material properties), simply supported, rectangular plates under surface loads, an extension of Pagano's previous solution [37,38] to the FGM case. The homogeneous solution in a single FGM plate is obtained in terms of a new and simple formalism similar to the Stroh formalism [39–41]. Solutions for the corresponding multilayered FGM plates are obtained using the propagator matrix method [42,43]. To the best of the author's knowledge, it is the first time that an anisotropic elastic FGM plate under simply supported edge conditions is studied analytically. Since the present solutions are exact, they can serve as benchmarks to various numerical methods, such as the finite and boundary element methods [44,45], used for the modeling of FGM composite structures.

As numerical illustrations, a single FGM plate and a bi-layer plate with an FGM layer overlying a homogeneous layer (named FGM/homo bi-layer plate) are analyzed. For both cases, a simple surface load is applied on the top surface of the plate. Numerical results are given for the variation of the displacements and stresses along the thickness direction of the plate for five different exponential factor values (i.e., $\eta = -1$, -0.5, 0, 0.5, 1, as defined below). Typical features observed from these numerical results should be of special interest to the design of FGM composite laminates. In particular, our numerical examples clearly show that with a suitable lay-up and an exponential factor η for the FGM, one could achieve an optimal design for the FGM composite laminates.

PROBLEM DESCRIPTION AND BASIC EQUATIONS

Let us consider an anisotropic, linearly elastic, and layered rectangular FGM plate with horizontal dimensions L_x and L_y and thickness H (in the vertical direction). The four sides of the plate are simply supported. Each layer of the plate can be homogeneous or FGM with exponentially varying material properties. A Cartesian coordinate system (x, y, z) is attached to the plate in such a way that its origin is at one of the four corners on the bottom surface and the plate is in the positive z-region. Only surface loading will be considered, while internal loading case can be treated similarly as in Pan [46]. Without loss of generality, we also assume that the surface load is applied on the top surface of the plate.

The constitutive relation for each layer can be written as

$$\sigma_i = C_{ik}\gamma_k \tag{1}$$

where σ_i are the stress, γ_i the strain, and C_{ij} the elastic stiffness matrix.

For an FGM layer with exponentially varying material properties in the z-direction, the elastic stiffness matrix in Equation (1) can be expressed as

$$C_{ik}(z) = C^0_{ik}e^{\eta z} \tag{2}$$

where η is the exponential factor characterizing the degree of material gradient in the z-direction. It is further noted that the exponential factor η has the dimension $1/L$, where L is the characteristic length of the problem. Figure 1 illustrates the variation of the exponential function $e^{\eta z}$ along the z-direction for five different η values ($=-1, -0.5, 0, 0.5, 1$).

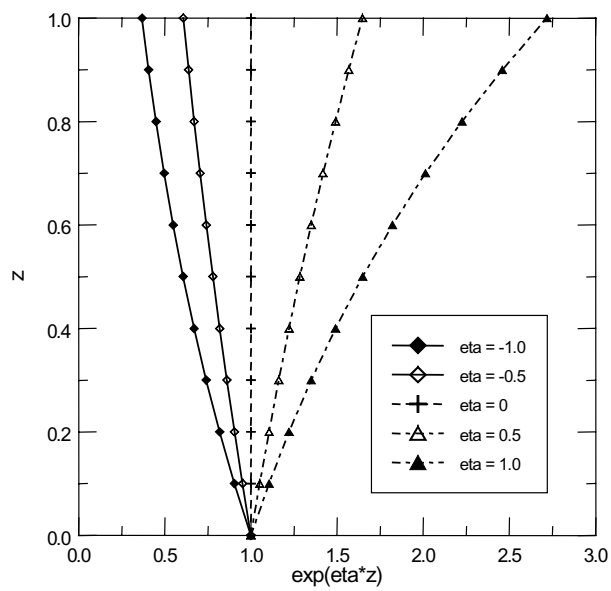

Figure 1. *Variation of exponential function $e^{\eta z}$ over $z\in[0,1]$ for factor $\eta=-1, -0.5, 0, 0.5$, and 1 (z in m and η in 1/m).*

We remark that $\eta = 0$ corresponds to the homogeneous case, $\eta < 0$ to the graded soft material, and $\eta > 0$ to the graded stiff material.

For an orthotropic elastic solid, the stiffness matrix in Equation (1) is reduced to

$$[C] = \begin{bmatrix} C_{11} & C_{12} & C_{13} & 0 & 0 & 0 \\ & C_{22} & C_{23} & 0 & 0 & 0 \\ & & C_{33} & 0 & 0 & 0 \\ & & & C_{44} & 0 & 0 \\ & \text{Sym} & & & C_{55} & 0 \\ & & & & & C_{66} \end{bmatrix} \tag{3}$$

The other two sets of equations are the strain (using tensor symbol γ_{ik})–displacement relation

$$\gamma_{ij} = 0.5(u_{i,j} + u_{j,i}) \tag{4}$$

with u_i being the displacement; and the equations of equilibrium

$$\sigma_{ij,j} + f_i = 0 \tag{5}$$

with f_i being the body force.

GENERAL SOLUTIONS

For a simply supported FGM plate, we seek the solution of the displacement vector in the form of

$$u \equiv \begin{bmatrix} u_x \\ u_y \\ u_z \end{bmatrix} = e^{sz} \begin{bmatrix} a_1 \cos px \sin qy \\ a_2 \sin px \cos qy \\ a_3 \sin px \sin qy \end{bmatrix} \tag{6}$$

where

$$p = n\pi/L_x, \quad q = m\pi/L_y \tag{7}$$

and n and m are two positive integers.

Substitution of Equation (6) into the strain–displacement relation (4), the constitutive relation (2), and finally into the equations of equilibrium (5) with zero body force, yields the following eigenequation

$$[\boldsymbol{Q} - \eta \boldsymbol{R}^{\mathrm{t}} + s(\boldsymbol{R} - \boldsymbol{R}^{\mathrm{t}} + \eta \boldsymbol{T}) + s^2 \boldsymbol{T}]\boldsymbol{a} = 0 \tag{8}$$

where superscript t denotes the transpose of matrix. Also in Equation (8),

$$\boldsymbol{a} = [a_1, a_2, a_3]^{\mathrm{t}} \tag{9}$$

$$\boldsymbol{R} = \begin{bmatrix} 0 & 0 & pC_{13}^0 \\ 0 & 0 & qC_{23}^0 \\ -pC_{55}^0 & -qC_{44}^0 & 0 \end{bmatrix}, \qquad \boldsymbol{T} = \begin{bmatrix} C_{55}^0 & 0 & 0 \\ 0 & C_{44}^0 & 0 \\ 0 & 0 & C_{33}^0 \end{bmatrix} \tag{10}$$

$$\boldsymbol{Q} = \begin{bmatrix} -(C_{11}^0 p^2 + C_{66}^0 q^2) & -pq(C_{12}^0 + C_{66}^0) & 0 \\ -pq(C_{12}^0 + C_{66}^0) & -(C_{66}^0 p^2 + C_{22}^0 q^2) & 0 \\ 0 & 0 & -(C_{55}^0 p^2 + C_{44}^0 q^2) \end{bmatrix} \tag{11}$$

Equation (8) is a new eigenequation for the FGM, and when $\eta = 0$, is reduced to the eigenequation for the corresponding homogeneous case [46].

Taking into consideration the simply supported edge conditions, along with the exponential variation of the stiffness matrix described by Equation (2), the traction vector can then be assumed as

$$\boldsymbol{t} \equiv \begin{bmatrix} \sigma_{xz} \\ \sigma_{yz} \\ \sigma_{zz} \end{bmatrix} = e^{(s+\eta)z} \begin{bmatrix} b_1 \cos px \sin qy \\ b_2 \sin px \cos qy \\ b_3 \sin px \sin qy \end{bmatrix} \tag{12}$$

To find the relation between a_i in Equation (6) and b_i in Equation (12), we first take the derivatives of the displacement (6) to obtain the strain field; we then substitute the result into Equations (1) and (2) to derive the stress field. Comparison of the coefficients of the same trigonometric functions finally gives us the following relation between the vectors $\boldsymbol{a}$ and $\boldsymbol{b}$

$$\boldsymbol{b} = (-\boldsymbol{R}^{\mathrm{t}} + s\boldsymbol{T})\boldsymbol{a} \tag{13}$$

with

$$\boldsymbol{b} = [b_1, b_2, b_3]^{\mathrm{t}} \tag{14}$$

Similarly, the in-plane stresses can be expressed as

$$\begin{bmatrix} \sigma_{xx} \\ \sigma_{xy} \\ \sigma_{yy} \end{bmatrix} = e^{(s+\eta)z} \begin{bmatrix} c_1 \sin px \sin qy \\ c_2 \cos px \cos qy \\ c_3 \sin px \sin qy \end{bmatrix} \tag{15}$$

where

$$\begin{bmatrix} c_1 \\ c_2 \\ c_3 \end{bmatrix} = \begin{bmatrix} -C_{11}^0 p & -C_{12}^0 q & C_{13}^0 s \\ C_{66}^0 q & C_{66}^0 p & 0 \\ -C_{12}^0 p & -C_{22}^0 q & C_{23}^0 s \end{bmatrix} \begin{bmatrix} a_1 \\ a_2 \\ a_3 \end{bmatrix} \tag{16}$$

In Pan [46], we have discussed the distinguished structure of an equation similar to Equation (8), and its solution for the homogeneous material case. Here, we further remark that, due to the involvement of the exponential factor η in Equation (8), certain features

discussed in [40] and [46] do not hold for the present FGM case. However, the following two features are still useful in the analysis: (1) If s is an eigenvalue of Equation (8), so is $-s$; and (2) If s is a complex (or purely imaginary) eigenvalue, then its complex conjugate is also an eigenvalue since all the coefficient matrices in Equation (8) are real.

With the aid of Equation (13), Equation (8) can now be recast as a 6×6 linear eigensystem

$$\boldsymbol{N}\begin{bmatrix}\boldsymbol{a}\\ \boldsymbol{b}\end{bmatrix} = s\begin{bmatrix}\boldsymbol{a}\\ \boldsymbol{b}\end{bmatrix} \tag{17}$$

where

$$\boldsymbol{N} = \begin{bmatrix}\boldsymbol{T}^{-1}\boldsymbol{R}^{\mathrm{t}} & \boldsymbol{T}^{-1}\\ -\boldsymbol{Q} - \boldsymbol{R}\boldsymbol{T}^{-1}\boldsymbol{R}^{\mathrm{t}} & -\boldsymbol{R}\boldsymbol{T}^{-1} - \eta\boldsymbol{I}\end{bmatrix} \tag{18}$$

with $\boldsymbol{I}$ being a 3×3 unit matrix.

It is of particular interest to notice that the only difference between the present matrix $\boldsymbol{N}$ for the FGM case and that for the homogeneous material case [46] is the involvement of the exponential factor η. However, because of this difference, the eigenpairs of Equation (17) are completely different from those corresponding to the homogeneous material case. Thus, the structure of the solution to Equation (17) is different from that in [40] or [46].

Depending upon the given material property, the six eigenvalues of Equation (17) may not be distinct. Should repeated roots occur, a slight change in the material constants would result in distinct roots with negligible error [47] so that the following simple solution structure can be applied to any material. Let us assume that the first three eigenvalues have positive real parts (if the root is purely imaginary, we then pick up the one with positive imaginary part) and the rest have opposite signs to the first three. We distinguish the corresponding 6 eigenvectors by attaching a subscript to $\boldsymbol{a}$ and $\boldsymbol{b}$. Then the general solutions for the displacement and traction vectors, expressed by Equations (6) and (12), are derived as (taking the z-dependent factor only)

$$\begin{bmatrix}\boldsymbol{u}\\ \boldsymbol{t}\end{bmatrix} = \begin{bmatrix}\boldsymbol{A}_1\langle e^{s^*z}\rangle & \boldsymbol{A}_2\langle e^{-s^*z}\rangle\\ \boldsymbol{B}_1\langle e^{(s^*+\eta)z}\rangle & \boldsymbol{B}_2\langle e^{(-s^*+\eta)z}\rangle\end{bmatrix}\begin{bmatrix}\boldsymbol{K}_1\\ \boldsymbol{K}_2\end{bmatrix} \tag{19}$$

where

$$\begin{aligned}\boldsymbol{A}_1 &= [\boldsymbol{a}_1, \boldsymbol{a}_2, \boldsymbol{a}_3], \quad \boldsymbol{A}_2 = [\boldsymbol{a}_4, \boldsymbol{a}_5, \boldsymbol{a}_6]\\ \boldsymbol{B}_1 &= [\boldsymbol{b}_1, \boldsymbol{b}_2, \boldsymbol{b}_3], \quad \boldsymbol{B}_2 = [\boldsymbol{b}_4, \boldsymbol{b}_5, \boldsymbol{b}_6]\\ \langle e^{s^*z}\rangle &= \mathrm{diag}[e^{s_1z}, e^{s_2z}, e^{s_3z}]\end{aligned} \tag{20}$$

and $\boldsymbol{K}_1$ and $\boldsymbol{K}_2$ are two 3×1 complex constant column matrices to be determined. In Equation (20), the column matrices $\boldsymbol{a}_i$ and $\boldsymbol{b}_i$, defined as

$$\begin{aligned}\boldsymbol{a}_i &= [a_{1i}, a_{2i}, a_{3i}]^{\mathrm{t}}\\ \boldsymbol{b}_i &= [b_{1i}, b_{2i}, b_{3i}]^{\mathrm{t}}\end{aligned} \tag{21}$$

are the eigenvectors of Equation (17), corresponding to the eigenvalue s_i ($i=1, 2, 3$); whilst for $i=4, 5, 6$ the column matrices $\boldsymbol{a}_i$ and $\boldsymbol{b}_i$ are the eigenvectors corresponding to the eigenvalue $-s_{i-3}$.

Equation (19) is a general solution for an FGM plate under simply supported edge conditions of a certain type. We should also point out that only the real part of the right-hand side of Equation (19) is chosen for the displacement and traction vector solutions. We further remark that, when $\eta=0$, this equation reduces to the solution for the corresponding homogeneous material case [37,38,46]. With Equation (19) serving as a general solution for the FGM plate, solutions for the corresponding multilayered FGM plate can be obtained using the continuity conditions along the interface and the boundary conditions on the top and bottom surfaces of the multilayered FGM plate. In doing so, a system of linear equations for the unknowns can be formed and solved [38,48]. Alternatively, the propagator matrix method can be utilized [42,43,46] which can substantially simplify the final solution, in particular, when the FGM plate consists of many layers. These analytical results could be beneficial to the design analysis using the thin FGM layer as coating material to protect the core and inner structures.

Before carrying out numerical studies using the present formulation, we emphasize again that the present solution is valid for any integers n and m as defined by Equation (7). In other words, the solution we have derived can be regarded as for one of the terms in a Fourier series expansion. Because of the linearity, the solution corresponding to a general loading (uniform or point loading) can be obtained by expanding the loading as a finite double Fourier series [49,50] and adding the responses together term by term.

NUMERICAL EXAMPLES

As the first example, let us consider a single FGM plate of orthotropy. The constant factors of the material properties (elastic modulus E, shear modulus G, and Poisson's ratios ν) are taken from Pagano [38]

$$\begin{aligned} E_L &= 25\times 10^6 \text{ psi} \qquad E_T = 10^6 \text{ psi} \\ G_{LT} &= 0.5\times 10^6 \text{ psi} \qquad G_{TT} = 0.2\times 10^6 \text{ psi} \\ \nu_{LT} &= \nu_{TT} = 0.25 \end{aligned} \tag{22}$$

where L (different from the length scale L used elsewhere in this paper) denotes the direction parallel to the fibers and T the transverse direction. Also, ν_{LT} is the Poisson's ratio measuring strain in the T-direction under the uniaxial normal stress in the L-direction. In the examples, L is chosen to be along the y-direction. Therefore, the constant stiffness matrix in Equation (2) in the (x, y, z)-coordinates can be expressed as

$$C_{ij}^0 = \begin{bmatrix} 7.3802 & 2.3121 & 1.8682 & 0 & 0 & 0 \\ & 173.406 & 2.3121 & 0 & 0 & 0 \\ & & 7.3802 & 0 & 0 & 0 \\ & & & 3.445 & 0 & 0 \\ & \text{Sym} & & & 1.378 & 0 \\ & & & & & 3.445 \end{bmatrix} (10^9 \text{ N/m}^2) \tag{23}$$

We also assume that the dimensions of the plate are $L_x \times L_y \times H = 1 \times 1 \times 1\,\mathrm{m}^3$, and a traction in the z-direction is applied on the top surface of the plate $z = H$, as given by

$$t(H) = [0, 0, \sigma_0 \sin px \sin qy]^{\mathrm{t}} \tag{24}$$

with $m = n = 1$ (i.e., $p = \pi/L_x$, $q = \pi/L_y$) and $\sigma_0 = 1\,\mathrm{N/m}^2$. The bottom surface is assumed to be traction-free. Responses are calculated in the thickness direction, with fixed horizontal coordinates (x, y) at $(0.75L_x, 0.25L_y)$.

Figure 2(a)–(c) show the variation of the displacement components (u_x, u_y, and u_z) along the thickness direction of the FGM plate. Numerical values are also given in Table 1 at $z = 0$ and 1.0 m for all three displacement components and also at $z = 0.5$ m for u_z. It is observed that on the top and bottom surfaces, the magnitudes of the horizontal displacements (i.e., u_x and u_y) decrease with increasing exponential factor η (i.e., η increases from -1 to 1, with $\eta = 0$ corresponding to the homogeneous case). This is what we expected: a graded stiff material ($\eta > 0$) will be hard to deform. Furthermore, since on the top surface the horizontal displacements are negative, while on the bottom surface they are positive, there is a location within the plate where curves intersect each other. This location is roughly at $z = 0.4$ m for u_x and at $z = 0.2$ m for u_y. The distribution of u_z is given in Figure 2(c), where again as we can see that the magnitude of u_z decreases with increasing exponential factor η.

Shown in Figure 3(a)–(f) are the variations of the stress components σ_{xx}, σ_{yy}, σ_{zz}, σ_{yz}, σ_{zx}, and σ_{xy} along the thickness direction of the plate. Numerical values are also given in

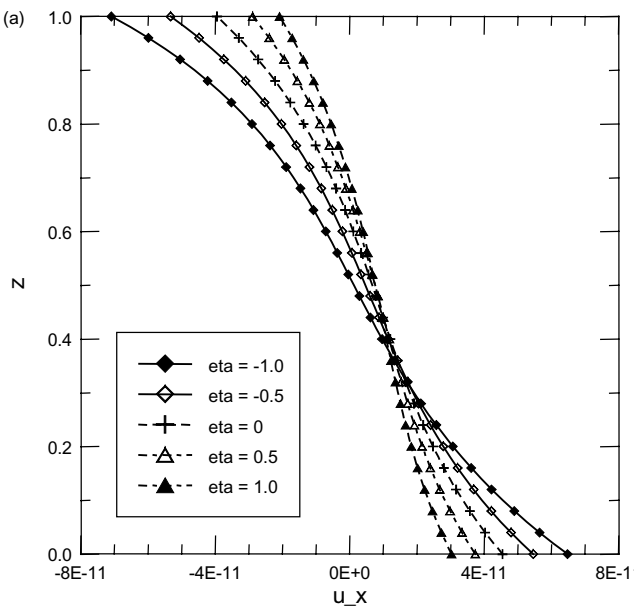

Figure 2. *(a) Variation of displacement component u_x along the thickness direction in single FGM plate for factor $\eta = -1, -0.5, 0, 0.5$, and 1 (u_x in m and η in 1/m); (b) Variation of displacement component u_y along the thickness direction in single FGM plate for factor $\eta = -1, -0.5, 0, 0.5$, and 1 (u_y in m and η in 1/m); (c) Variation of displacement component u_z along the thickness direction in single FGM plate for factor $\eta = -1, -0.5, 0, 0.5$, and 1 (u_z in m and η in 1/m).*

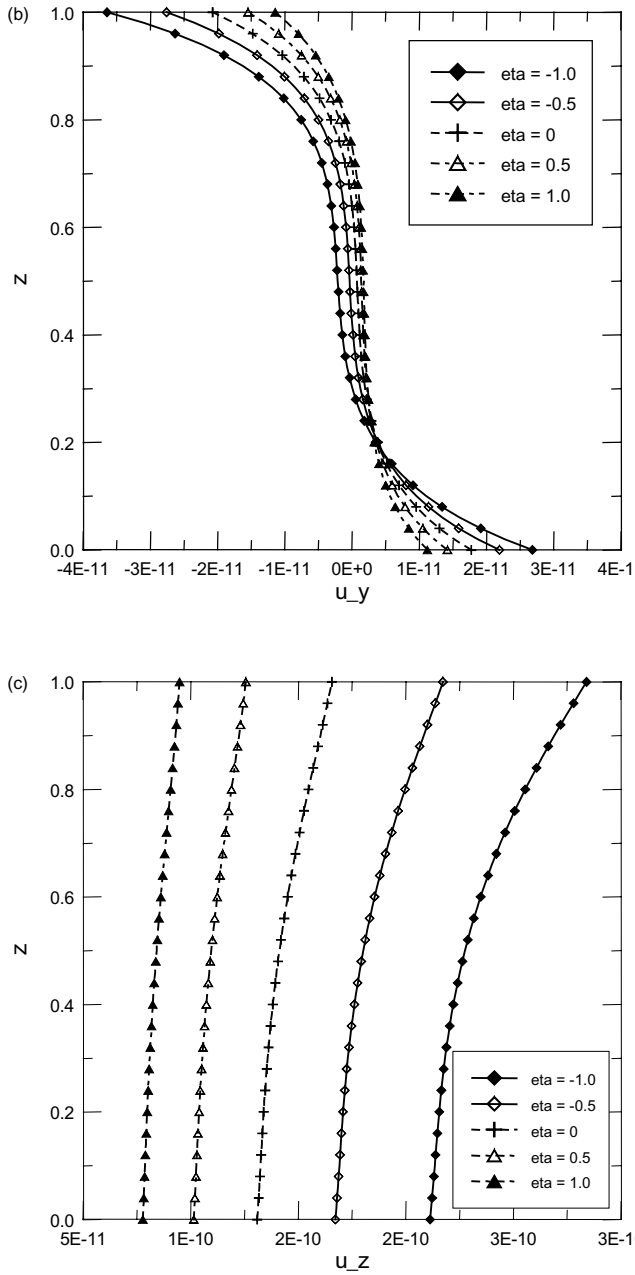

Figure 2. *Continued.*

Table 2 for the normal stress components σ_{xx} and σ_{yy} at $z = 0$, 0.5 m and 1.0 m, and for the normal stress component σ_{zz} at $z = 0.5$ m. Table 3 lists numerical values for the shear stress components σ_{yz} and σ_{zx} at $z = 0.3$ m and 0.7 m, and the shear stress component σ_{xy} at $z = 0$, 0.5 m and 1.0 m.

It is interesting that while for the horizontal displacements there is only one location in the z-direction where two curves intersect each other, for the horizontal stresses (σ_{xx}, σ_{yy}, and σ_{xy}) there are two locations along the z-direction where curves intersect each other (Figure 3(a), (b) and (f)). For σ_{xx} and σ_{xy}, these intercept locations are roughly at $z = 0.2$ m and 0.8 m, whilst for σ_{yy}, they are at $z = 0.15$ m and $z = 0.85$ m. It is also observed that on the top surface, σ_{xx} and σ_{yy} are tensile, and σ_{xy} is negative; on the bottom surface, on the other hand, σ_{xx} and σ_{yy} are compressive, and σ_{xy} is positive. While σ_{xx} and σ_{xy} have the same

Table 1. Displacements (in 10^{-11} m) for different η at different z-levels (in m).

		$\eta = -1$	$\eta = -0.5$	$\eta = 0$	$\eta = 0.5$	$\eta = 1$
u_x	$z = 0.0$	6.48758	5.46503	4.54910	3.74002	3.03593
	$z = 1.0$	−7.09212	−5.32779	−3.94922	−2.88987	−2.08884
u_y	$z = 0.0$	2.68529	2.19394	1.77373	1.41893	1.12321
	$z = 1.0$	−3.64298	−2.75880	−2.07327	−1.54532	−1.14191
u_z	$z = 0.0$	21.1343	16.7250	13.0954	10.1442	7.77486
	$z = 0.5$	22.7567	18.0238	14.1290	10.9611	8.41538
	$z = 1.0$	28.4116	21.7324	16.5679	12.5702	9.48080

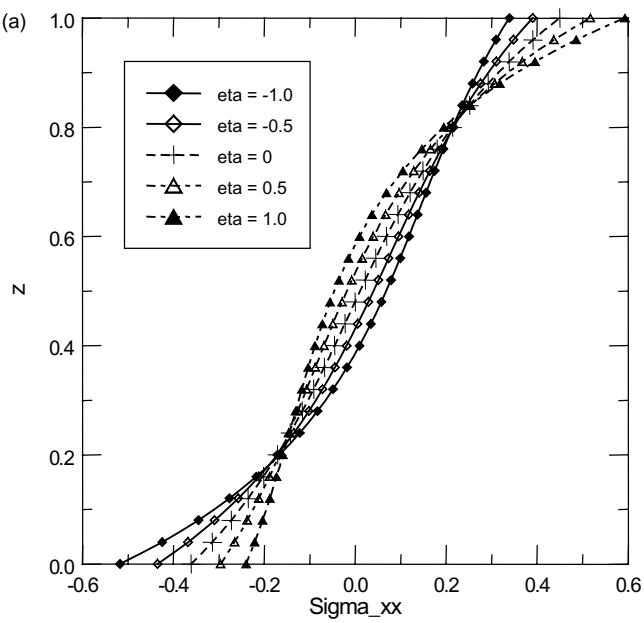

Figure 3. *(a) Variation of stress component σ_{xx} along the thickness direction in single FGM plate for factor $\eta = -1$, -0.5, 0, 0.5, and 1 (σ_{xx} in N/m^2 and η in 1/m); (b) Variation of stress component σ_{yy} along the thickness direction in single FGM plate for factor $\eta = -1$, -0.5, 0, 0.5, and 1 (σ_{yy} in N/m^2 and η in 1/m); (c) Variation of stress component σ_{zz} along the thickness direction in single FGM plate for factor $\eta = -1$, -0.5, 0, 0.5, and 1 (σ_{zz} in N/m^2 and η in 1/m); (d) Variation of stress component σ_{yz} along the thickness direction in single FGM plate for factor $\eta = -1$, -0.5, 0, 0.5, and 1 (σ_{yz} in N/m^2 and η in 1/m); (e) Variation of stress component σ_{zx} along the thickness direction in single FGM plate for factor $\eta = -1$, -0.5, 0, 0.5, and 1 (σ_{zx} in N/m^2 and η in 1/m); (f) Variation of stress component σ_{xy} along the thickness direction in single FGM plate for factor $\eta = -1$, -0.5, 0, 0.5, and 1 (σ_{xy} in N/m^2 and η in 1/m).*

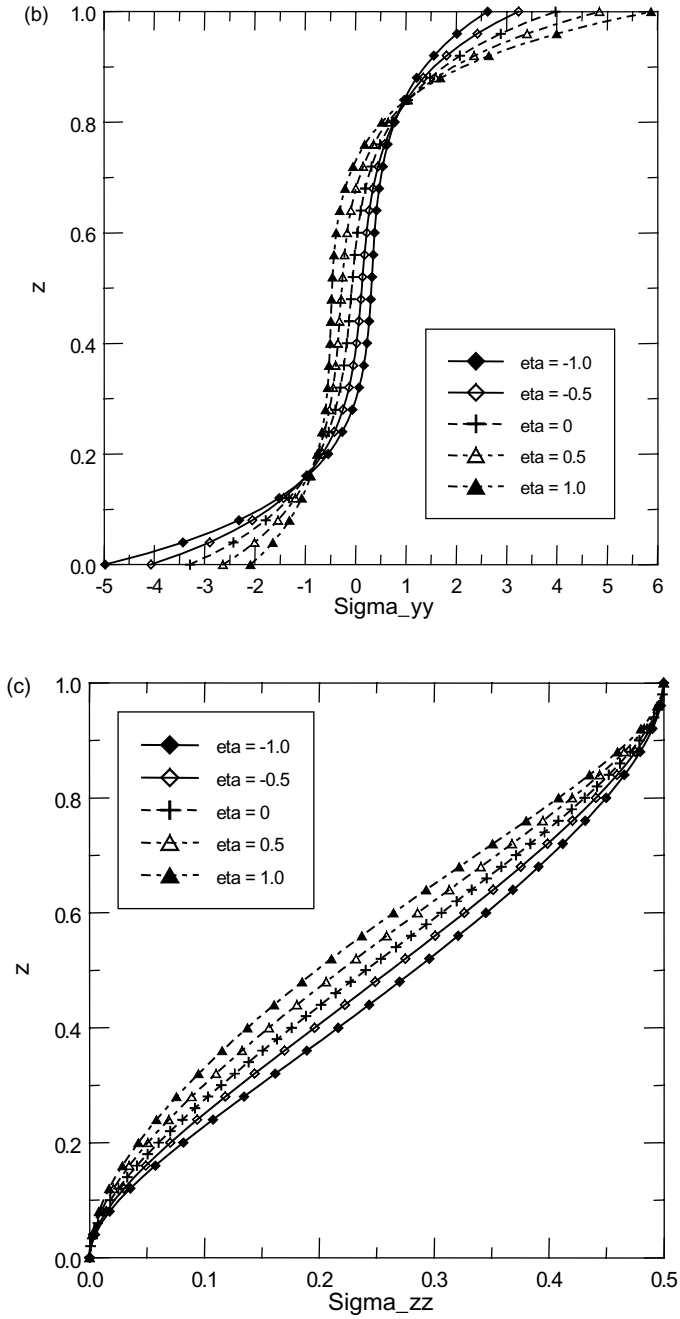

Figure 3. *Continued.*

magnitude, they both are one order small than σ_{yy}, due to the fact that the y-direction is along the fiber direction (Equations (22) and (23)). As for other shear stress components σ_{yz} and σ_{zx} (Figure 3(d) and (e)), we notice that the magnitude of σ_{yz}, which is in the same order of σ_{xy}, is much large than σ_{zx} (about 4 times). However, they both show similar variation

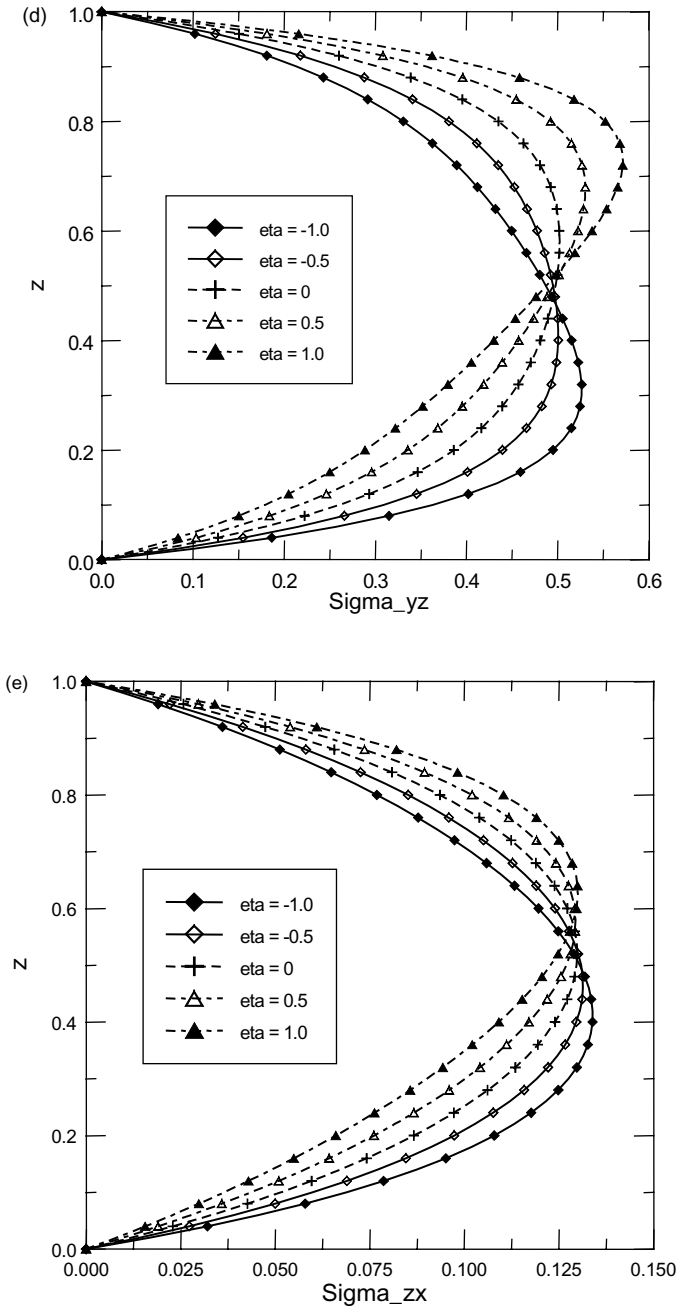

Figure 3. *Continued.*

along the z-direction; that is, with the increasing exponential factor η, their magnitude increases in the bottom half ($z < 0.5$ m) but decreases in the top half of the plate ($z > 0.5$ m).

Naturally, one would ask: how could these displacement and stress behaviors in the FGM plate be applicable or beneficial to the design of FGMs? Actually, an in-depth study

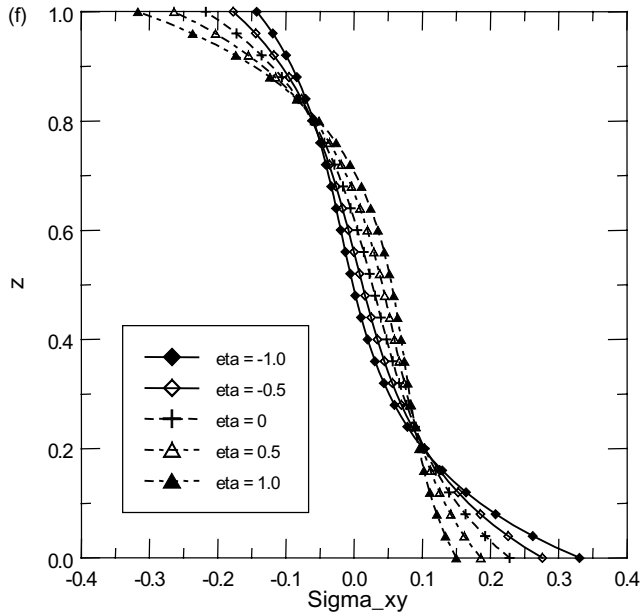

Figure 3. *Continued.*

Table 2. Normal stresses (in N/m^2) for different η at different z-levels (in m).

		$\eta=-1$	$\eta=-0.5$	$\eta=0$	$\eta=0.5$	$\eta=1$
σ_{xx}	$z=0.0$	−0.517825	−0.434976	−0.361124	−0.296185	−0.239909
	$z=0.5$	0.068474	0.040066	0.010842	−0.018116	−0.045730
	$z=1.0$	0.339523	0.390569	0.449718	0.517278	0.593411
σ_{yy}	$z=0.0$	−4.97318	−4.06616	−3.28973	−2.63350	−2.08601
	$z=0.5$	0.316919	0.125018	−0.073896	−0.273434	−0.467122
	$z=1.0$	2.62729	3.24093	3.97718	4.85003	5.87242
σ_{zz}	$z=0.5$	0.283086	0.262026	0.240560	0.219018	0.197730

Table 3. Shear stresses (in N/m^2) for different η at different z-levels (in m).

		$\eta=-1$	$\eta=-0.5$	$\eta=0$	$\eta=0.5$	$\eta=1$
σ_{yz}	$z=0.3$	0.526202	0.488592	0.448736	0.407614	0.366208
	$z=0.7$	0.401106	0.444140	0.487241	0.529387	0.569522
σ_{zx}	$z=0.3$	0.127576	0.119228	0.110029	0.100224	0.090089
	$z=0.7$	0.101806	0.109083	0.115878	0.121939	0.127046
σ_{xy}	$z=0.0$	0.330920	0.276305	0.228102	0.186114	0.150045
	$z=0.5$	−0.001847	0.012356	0.027015	0.041542	0.055348
	$z=1.0$	−0.142472	−0.176944	−0.217267	−0.263801	−0.316823

on the normal stresses σ_{xx} and σ_{yy}, in particular σ_{yy}, on the surfaces of the FGM plate reveals some interesting features which might be directly useful to the design of FGMs. From Figure 3(a) and (b), one observes that, the tensile stress on the top surface can be reduced substantially by using a graded soft material (i.e., $\eta<0$); on the other hand

however, the compressive stress on the bottom surface will be increased (in approximately the same ratio as on the top surface for the tensile stress). Similarly, a substantial reduction on the compressive stress on the bottom surface can be achieved by using a graded stiff material, which on the other hand increases the tensile stress on the top surface. We remark that our results are for a single FGM plate; a multilayered FGM laminate could be designed to reduce the variation of the normal stress along one of the surfaces of the FGM (actually it is the interface between the FGM and the plate). Therefore, it is possible that, by adjusting the exponential factor η, one can achieve an optimal design for the FGM composite. To further elaborate our points, numerical modeling has been also carried out for a bi-layer plate made of an FGM layer overlying a homogeneous layer (i.e., the FGM/homo bi-layer plate), which is explained below in certain details.

For the second example, the geometry of the FGM/homo bi-layer plate is very similar to the single FGM plate. The dimensions of the plate are still $L_x \times L_y \times H = 1 \times 1 \times 1\,\mathrm{m}^3$. However, the bottom part of the FGM/homo bi-layer plate, i.e., $0 \le z \le 0.7\,\mathrm{m}$, is now a homogeneous layer with elastic constants being given by Equation (23); while for its top part, i.e., $0.7 \le z \le 1\,\mathrm{m}$, we use the FGM material given by

$$C_{ik}(z) = C_{ik}^0 e^{\eta(z-0.7)} \tag{25}$$

In so doing, the material properties (and thus the displacement and stress components) are continuous along the interface between the FGM layer and the homogenous layer. Again, the bottom surface ($z = 0$) is traction free, and the top surface ($z = 1\,\mathrm{m}$) is under the load given by Equation (24). For $m = n = 1$ (i.e., $p = \pi/L_x$, $q = \pi/L_y$) and $\sigma_0 = 1\,\mathrm{N/m}^2$, we calculated the displacement and stress fields in the thickness direction, with fixed horizontal coordinates $(x, y) = (0.75L_x, 0.25L_y)$.

Shown in Figure 4(a) and (b) are the variations of the normal stress components σ_{xx} and σ_{yy} along the thickness direction of the FGM/homo bi-layer plate for the five different exponential factors $\eta = (-1, -0.5, 0, 0.5, 1)$. It is clearly shown that, using a graded soft layer (i.e., $\eta < 0$), the tensile stress on the top surface of the FGM/homo bi-layer plate can be reduced by 13% for σ_{xx} and 18% for σ_{yy}, while at the same time the stress variation along the interface ($z = 0.7\,\mathrm{m}$) is minor. In particular, the compressive stresses along the bottom surface are nearly the same for the five different exponential factor values. Similarly, a bi-layer plate with a homogeneous layer overlying a graded stiff layer, i.e., the homo/FGM bi-layer, will reduce the compressive stress along the bottom surface of the bi-layer plate.

CONCLUSIONS

In this paper, we have derived the exact solution for 3D anisotropic, linearly elastic, and FGM rectangular composite laminates under simply supported edge conditions. We expressed the solution in terms of a simple formalism similar to the Stroh formalism. The composite laminates can be made of multilayered FGMs with their properties varying exponentially in the thickness direction. When the exponential factor $\eta = 0$, the present solution is reduced to Pagano's solution [37,38].

Numerical results are also presented for a single FGM plate and an FGM/homo bi-layer plate, both under a simple load on the top surface. Several interesting features

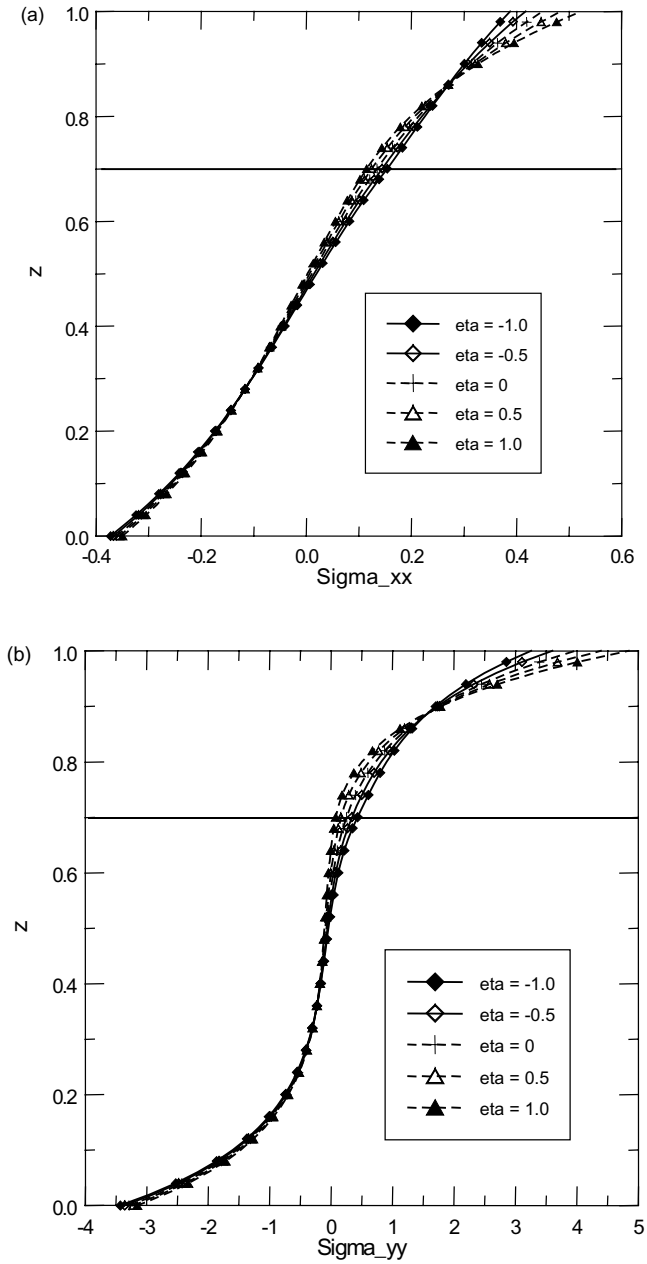

Figure 4. *(a) Variation of stress component σ_{xx} along the thickness direction in FGM/homo bi-layer plate for factor $\eta = -1$, -0.5, 0, 0.5, and 1 (σ_{xx} in N/m^2 and η in 1/m); (b) Variation of stress component σ_{yy} along the thickness direction in FGM/homo bi-layer plate for factor $\eta = -1$, -0.5, 0, 0.5, and 1 (σ_{yy} in N/m^2 and η in 1/m).*

were observed for the displacement and stress variations within the FGM plates. In particular, it is clearly shown that with a suitable FGM layer bonded to a homogeneous layer, one could reduce the tensile stress on the top surface (for the FGM/homo bi-layer) or the compressive stress on the bottom surface (for the homo/FGM bi-layer) of the

bi-layer plate. Therefore, using an FGM layer with a suitably selected exponential factor η, an optimal design for FGM laminates could be achieved for the best performance. We finally remark that, although the FGM used in this study is hypothetical, fabrication of anisotropic FGM with controlled variables is possible [51].

ACKNOWLEDGEMENTS

The author would like to thank the reviewer for his/her constructive comments and suggestions. He is also greatly indebted to Dr. Pagano who has kindly read and corrected the paper, and offered various instructive comments. The author therefore dedicates this paper to Dr. Pagano on the occasion of his retirement from the AFRL.

REFERENCES

1. Pipes, R.B. and Pagano, N.J. (1970). Interlaminar Stresses in Composite Laminates under Uniform Axial Extensions, *Journal of Composite Materials*, **4**: 538–548.
2. Pipes, R.B. and Pagano, N.J. (1974). Interlaminar Stresses in Composite Laminates – An Approximate Elasticity Solution, *Journal of Applied Mechanics*, **41**: 668–672.
3. Pagano, N.J. (1974). On the Calculation of Interlaminar Normal Stress in Composite Laminate, *Journal of Composite Materials*, **8**: 65–81.
4. Erdogan, F. (1995). Fracture Mechanics of Functionally Graded Materials, *Composites Engineering*, **5**: 753–770.
5. Suresh, S. and Mortensen, A. (1998). *Fundamentals of Functionally Graded Materials*, Institute of Materials, London.
6. Suresh, S. (2001). Graded Materials for Resistance to Contact Deformation and Damage, *Science*, **292**: 2447–2451.
7. Niino, M. and Maeda, S. (1990). Recent Development Status of Functionally Graded Materials, *I. S. I. J. Int.*, **30**: 699–703.
8. Delale, F. and Erdogan, F. (1983). The Crack Problem for a Nonhomogeneous Plane, *J. Appl. Mech.*, **50**: 609–614.
9. Delale, F. and Erdogan, F. (1988). Interface Crack in a Non-homogeneous Elastic Medium, *Int. J. Eng. Sci.*, **26**: 559–568.
10. Jin, Z.H. and Noda, N. (1994). Crack-tip Singular Fields in Nonhomogeneous Materials, *J. Appl. Mech.*, **61**: 738–740.
11. Jin, Z.H. and Batra, R.C. (1996). Some Basic Fracture Mechanics Concepts in Functionally Graded Materials, *J. Mech. Phys. Solids*, **44**: 1221–1235.
12. Aboudi, J., Pindera, M.J. and Arnold, S.M. (1995). Thermo-inelastic Response of Functionally Graded Composites, *Int. J. Solids and Structures*, **32**: 1675–1710.
13. Aboudi, J., Pindera, M.J. and Arnold, S.M. (1995). A Coupled Higher-order Theory for Functionally Graded Composites with Partial Homogenization, *Composites Engineering*, **52**: 771–792.
14. Aboudi, J., Pindera, M.J. and Arnold, S.M. (1997). Microstructural Optimization of Functionally Graded Composites Subjected to a Thermal Gradient via the Coupled Higher-order Theory, *Composites Part B-Engineering*, **28**: 93–108.
15. Aboudi, J., Pindera, M.J. and Arnold, S.M. (1999). Higher-order Theory for Functionally Graded Materials, *Composites Part B-Engineering*, **30**: 777–832.
16. Paulino, G.H. and Jin, Z.H. (2001). Correspondence Principle in Viscoelastic Functionally Graded Materials, *J. Appl. Mech.*, **68**: 129–132.

17. Paulino, G.H. and Jin, Z.H. (2001). Viscoelastic Functionally Graded Materials Subjected to Antiplane Shear Fracture, *J. Appl. Mech.*, **68**: 284–293.
18. Rousseau, C.E. and Tippur, H.V. (2002). Evaluation of Crack-tip Fields and Stress Intensity Factors in Functionally Graded Elastic Materials: Cracks Parallel to Elastic Gradient, *Int. J. Fracture*, **114**: 87–111.
19. Dolbow, J.E. and Gosz, M. (2002). On the Computation of Mixed-mode Stress Intensity Factors in Functionally Graded Materials, *Int. J. Solids Struct.*, **39**: 2557–2574.
20. Paulino, G.H. and Kim, J.H. (2002). Mixed-mode Fracture of Orthotropic Functionally Graded Materials Using the Finite Element Method, *Eng. Fract. Mech.*, **69**: 1557–1586.
21. Paulino, G.H. and Kim, J.H. (2002). Isoparametric Graded Finite Elements for Nonhomogeneous Isotropic and Orthotropic Materials, *J. Appl. Mech.*, **69**: 502–514.
22. Paulino, G.H. and Kim, J.H. (2002). Finite Element Evaluation of Mixed-mode Stress Intensity Factors in Functionally Graded Materials, *Int. J. Num. Meth. Eng.*, **53**: 1903–1935.
23. Jin, Z.H., Paulino, G.H. and Dodds, Jr. R.H. (2002). Finite Element Investigation of Quasi-static Crack Growth in Functionally Graded Materials Using a Novel Cohesive Zone Fracture Model, *J. Appl. Mech.*, **69**: 370–379.
24. Shbeeb, N.I., Binienda, W.K. and Kreider, K.L. (1999). Analysis of the Driving Forces for Multiple Cracks in Infinite Non-homogeneous Plate, Part I: Analysis, *J. Appl. Mech.*, **66**: 492–500.
25. Shbeeb, N.I., Binienda, W.K. and Kreider, K.L. (1999). Analysis of the Driving Forces for Multiple Cracks in Infinite Non-homogeneous Plate, Part II: Parametric Study, *J. Appl. Mech.*, **66**: 501–506.
26. Shbeeb, N.I., Binienda, W.K. and Kreider, K.L. (2000). Analysis of the Driving Force for a Generally Oriented Crack in a Functionally Graded Strip Sandwiched Between Two Homogeneous Half Planes, *Int. J. Fracture*, **104**: 23–50.
27. Dag, S. and Erdogan, F. (2002). A Surface Crack in a Graded Medium under General Loading Conditions, *J. Appl. Mech.*, **69**: 580–588.
28. Booker, J.R., Balaam, N.P. and Davis, E.H. (1985). The Behavior of an Elastic Non-homogeneous Half-Space. Part I – Line and Point Loads, *Int. J. Numer. Analy. Meth. Geomech.*, **9**: 353–367.
29. Ben-Menahem, A. (1987). Green's Tensor and its Potentials for Inhomogeneous Elastic Media, *Proc. R. Soc. Lond.*, **A409**: 287–327.
30. Giannakopoulos, A.E. and Suresh, S. (1997). Indentation of Solids with Gradients in Elastic Properties: Part I. Point Force, *Int. J. Solids Struct.*, **34**: 2357–2392.
31. Kim, K.S. and Noda, N. (2001). Green's Function Approach to Three-dimensional Heat Conduction Equation of Functionally Graded Materials, *J. Thermal Stresses*, **24**: 457–477.
32. Gray, L.J., Kaplan, T., Richardson, J.D., and Paulino, G.H. (2003). Green's Functions and Boundary Integral Analysis for Exponentially Graded Materials: Heat Conduction, *J. Appl. Mech.*, (in press).
33. Martin, P.A., Richardson, J.D., Gray, L.J. and Berger, J.R. (2002). On Green's Function for a Three-dimensional Exponentially-Graded Elastic Solid, *Proc. R. Soc. Lond.*, **A458**: 1931–1948.
34. Wang, C.D., Tzeng, C.S., Pan, E. and Liao, J.J. (2003). Displacements and Stresses due to a Vertical Point Load in an inhomogeneous Transversely Isotropic Half-space, *Int. J. Rock Mech. Min. Sci. & Geomech. Abstr.*, (in press).
35. Horgan, C.O. and Chan, A.M. (1999). The Pressurized Hollow Cylinder or Disk Problem for Functionally Graded Isotropic Linearly Elastic Materials, *J. Elasticity*, **55**: 43–59.
36. Vel, S.S. and Batra, R.C. (2002). Exact Solution for Thermoelastic Deformations of Functionally Graded Thick Rectangular Plates, *AIAA Journal*, **40**: 1421–1433.
37. Pagano, N.J. (1969). Exact Solutions for Composites in Cylindrical Bending, *Journal of Composite Materials*, **3**: 398–411.
38. Pagano, N.J. (1970). Exact Solutions for Rectangular Bidirectional Composites and Sandwich Plates, *Journal of Composite Materials*, **4**: 20–34.
39. Stroh, A.N. (1958). Dislocations and Cracks in Anisotropic Elasticity, *Phil. Mag.*, **3**: 625–646.
40. Ting, T.C.T. (1996). *Anisotropic Elasticity*, Oxford University Press, Oxford.

41. Ting, T.C.T. (2000). Recent Developments in Anisotropic Elasticity, *Int. J. Solids Structures*, **37**: 401–409.
42. Gilbert, F. and Backus, G. (1966). Propagator Matrices in Elastic Wave and Vibration Problems, *Geophys.*, **31**: 326–332.
43. Pan, E. (1997). Static Green's Functions in Multilayered Half Spaces, *Appl. Math. Modelling*, **21**: 509–521.
44. Ochoa, O.O. and Reddy, J.N. (1992). *Finite Element Analysis of Composite Laminates*, Kluwer Academic Publishers, Boston, MA.
45. Pan, E., Yang, B., Cai, G. and Yuan, F.G. (2001). Stress Analysis around Holes in Composite Laminates Using Boundary Element Method, *Eng. Anal. Bound. Elements*, **25**: 31–40.
46. Pan, E. (2001). Exact Solution for Simply Supported and Multilayered Magneto-Electro-Elastic Plates, *Journal of Applied Mechanics*, **68**: 608–618.
47. Pan, E. (1997). A General Boundary Element Analysis of 2-D Linear Elastic Fracture Mechanics, *Int. J. Fracture*, **88**: 41–59.
48. Heyliger, P. (1997). Exact Solutions for Simply Supported Laminated Piezoelectric Plates, *Journal of Applied Mechanics*, **64**: 299–306.
49. Timoshenko, S. and Woinowsky-Krieger, S. (1987). *Theory of Plates and Shells*, McGraw-Hill, New York.
50. Bisegna, P. and Maceri, F. (1996). An Exact Three-dimensional Solution for Simply Supported Rectangular Piezoelectric Plates, *J. Appl. Mech.*, **63**: 628–638.
51. Chatterjee, D.K., Ghosh, S.K. and Furlani, E.P. (1999). Controlled Composition and Crystallographic Changes in Forming Functionally Gradient Piezoelectric Transducer, U.S. Patent, No. 5,900,274.